Light scattering from an exploded lithium wire plasma*†

T. A. Leonard‡ and D. R. Bach

Nuclear Engineering Department, The University of Michigan, Ann Arbor, Michigan 48105
(Received 31 July 1972)

A thin lithium wire was extruded and exploded in vacuum and the resulting plasma was studied during the first 2 μsec of the discharge. Included in the study were scattering of a Q-switched ruby laser beam, high-speed streak photographs showing the laser-plasma interaction, and time-resolved emission spectra. The low pressure in the discharge chamber of 5×10^{-5} Torr prevented current shunting and also resulted in a "clean" lithium emission spectrum. The electron density calculated from mass conservation and temperature varied from 10^{17} to 10^{19} cm^{-3} as the plasma column oscillated in diameter. These densities matched those obtained from a Fresnel reflection model very well. Broadening or shifting of the scattered light was less than 1 A and the intensities yielded electron densities from 2×10^{19} to 10^{22} cm^{-3} when interpreted as cooperative electron scattering. The emission spectra from 3500 to 6900 Å showed three Li I, seven Li II, one Li III, and one unidentified line. The spectroscopic temperature obtained from various line ratios averaged about 4 eV, whereas the temperature found from a simple "snowplow" model analysis varied from 4 to 25 eV. The electron density measured by Stark broadening of emission lines compared well with the average density obtained through mass conservation.

I. INTRODUCTION

An exploded wire system provides a simple way of producing a plasma with a density comparable to that of the typical laser-produced plasma although the temperature is considerably lower. Unfortunately, there are few diagnostic methods for density and temperature measurements in these dense short-duration plasmas. Light scattering holds considerable promise but so far its use has been limited.[1–4]

The purpose of this investigation was to study light scattering in the high-density low-temperature plasma produced by an exploded wire (EW). Scattering theory has not been tested in this regime[5] but the increasing interest in dense laser-produced plasmas for controlled fusion makes this a topic of current interest. The only previous laser interaction studies with an EW plasma were limited to studies of absorption[6,7] and heating.[8]

Several light-scattering studies with laser-produced plasmas showed anomalously high electron densities when the scattering was interpreted as cooperative electron scattering.[9,10] It was suggested that the strong scattering was due to Fresnel reflection at the vacuum-plasma interface. In this experiment with an EW plasma, light scattering also gave anomalously high electron densities and, in fact, streak photographs showed that the interaction normally took place at the plasma edges.

Lithium was chosen as the wire material for its low atomic number and ease of extrusion. The EW apparatus used in this study and described in Sec. II was unique in that the lithium was extruded and exploded at a pressure of 5×10^{-5} Torr. The small wire size (0.0025 or 0.0075 cm in diameter) and high current gave strong pinching and a relatively high temperature for an EW plasma. The low pressure resulted in a clean lithium emission spectrum and in addition it prevented shunting of current around the wire by the surrounding gas. The entire wire was vaporized and ionized within 100 nsec.

The models used to extract densities and temperature from the data are described in Sec. III. Temperature was measured spectroscopically by the line ratio method and was also inferred from linear pinch dynamics and the measured total current flowing in the plasma. The number of neutrals and ions per unit length were deduced from mass conservation and the number of electrons was found by assuming Saha equilibrium.

The laser was usually Q switched at about 1 μsec when the discharge current had risen to 48 000 A. The plasma column disintegrated after 2 μsec and the scattered intensity dropped below the sensitivity of our detection system. An absolute calibration of the detectors was provided by observing Raleigh scattering in nitrogen.

II. EXPERIMENTAL APPARATUS

The main features of the equipment are shown in Fig. 1. The Korad K1-Q laser output was plane polarized in the vertical direction with scattered light observed at 90° in the horizontal plane. A 401-mm focal-length lens gave a 2-mm-diam beam at the plasma. Simple apertures at appropriate places, plus precautions in keeping the Brewster windows clean, were sufficient to keep 6943-Å stray light at the level of Rayleigh scattering from 760 Torr of nitrogen. A black cloth placed over the optical train to the spectrometer reduced stray light to less than 1% of the Rayleigh scattered light. This corresponded to an equivalent electron density for Thompson scattered light of 7.1×10^{14} cm^{-3} which was completely adequate for this experiment.

A photodiode was used to monitor the laser energy and a dull-black flat beam dump allowed easy monitoring of the transmitted beam by a second photodiode. The total energy, which was measured with a thermopile, was about 0.4 J with an average power of 20 MW or 6.7×10^{8} W/cm^2 at the plasma surface. The laser output was purposely kept low to avoid perturbing the plasma.

Mode hopping from shot to shot shifted the laser output by as much as 1 Å.[11] The purpose of the light delay shown in Fig. 1 was to monitor the wavelength and intensity of the original laser signal. It consisted of 190 ft of flexible glass fiber optics and had a total transmission of 8×10^{-6}.

The basic discharge circuit was described in a previous note[12] and consisted of a 14-μF condenser charged to 15 kV which was discharged through the wire with a spark-gap switch. The return current was symmetrically dis-

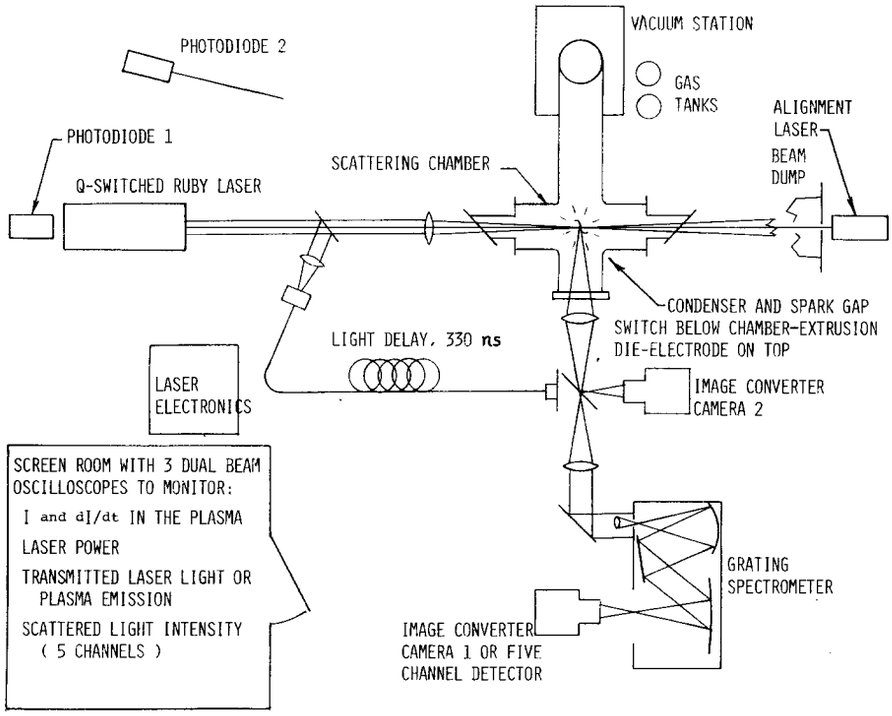

FIG. 1. Schematic layout of the equipment

posed about the wire. The peak current was 100 kA in the underdamped circuit with a quarter period of 3.1 μsec. The wire length was 5.2 cm.

The timing electronics consisted of transistorized delay units which drove 2D21 hydrogen thyratrons. The 2D21's provided + 300-V trigger pulses which were sufficient for starting the oscilloscopes and image-converter cameras. A 5C22 hydrogen thyratron was used to provide a – 10-kV pulse to trigger the spark-gap switch.

The extrusion die, which also served as an electrode to explode the wire, is shown in Fig. 2. The process of making the die and extruding the wire has been described previously.[13]

The diagnostic equipment consisted of two image-converter cameras (ICC), an $f/6.3$, $\frac{3}{4}$-m plane grating spectrometer, and a five-channel fiber-optics photomultiplier detector. ICC2 was used to obtain streak photographs of the expanding plasma column. A horizontal slit at the camera photocathode was imaged at the midpoint of the vertical wire. Streaking the slit vertically along the film gave a time history of the column diameter. A red bandpass filter allowed the scattered laser light to be seen in spite of the strong plasma emission.

ICC1 was used with the spectrometer to obtain time-resolved emission spectra and to look for wavelength structure in the scattered light. Sensitivity of the ICC and film was only sufficient to observe scattering stronger than 500 times Rayleigh scattering from 760 Torr of nitrogen which corresponded to an electron density of 7×10^{19} cm^{-3} if Thompson scattered. For this reason the five-channel detector was built to study the more weakly scattered light. Line driver amplifiers were used on each channel to drive the 20-ft cables to the oscilloscopes in the screen room. The amplifiers were transistorized and battery operated to minimize problems with electrical interference from the discharge.

III. RESULTS AND ANALYSIS

The virtues of using a low ambient pressure in the experiments were not immediately obvious. In fact it would have been more convenient to use a pressure

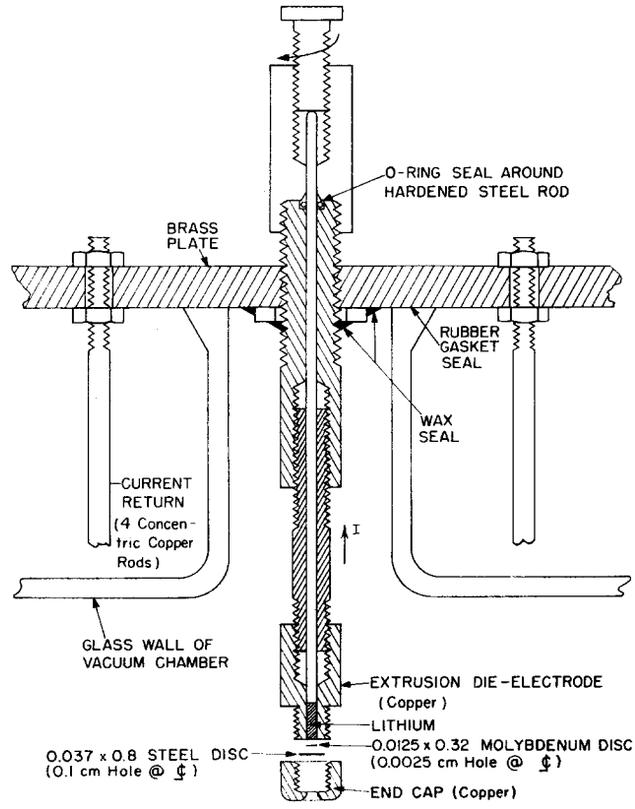

FIG. 2. Extrusion die-electrode assembly.

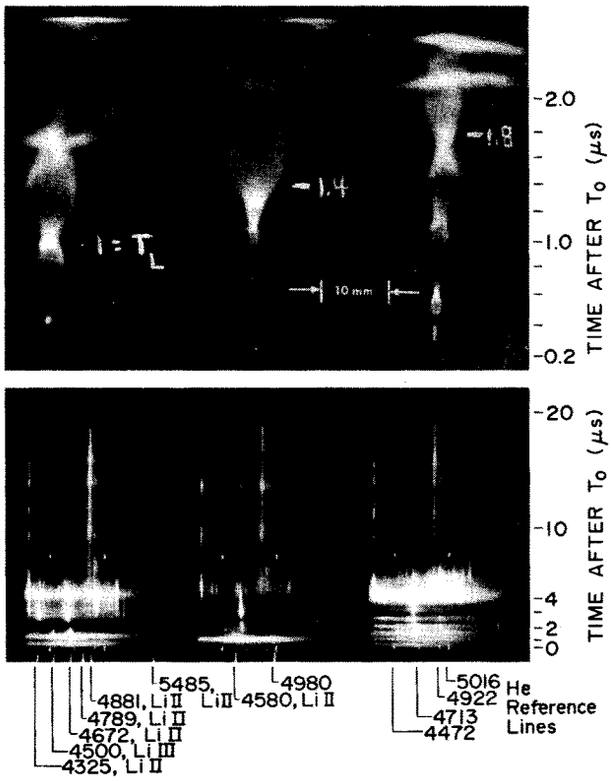

FIG. 3. Three examples of time-resolved emission spectra from 4250 to 5500 Å and the corresponding streak photographs. The wire diameter d was 0.0025 cm and the pressure was 5×10^{-5} Torr.

above 10^{-3} Torr since it resulted in a very "smooth" repeatable discharge. In contrast, pressures below about 0.5×10^{-3} Torr resulted in strong fluctuations in the rate of change of discharge current. Copious amounts of rf noise were produced in the plasma, and the scattered light intensity was weaker and less repeatable than at higher pressures.

The most reasonable explanation for stronger scattering above 10^{-3} Torr was failure of part of the wire to vaporize because of current shunting through the ambient gas.[14,15] This assumption was supported by framing pictures which showed emission from the surrounding gas at the higher pressure, whereas at lower pressures the only emission was from a distinct plasma column. The much stronger scattering at pressures above 10^{-3} Torr originated from the original wire location in the plasma. Cores have been seen in EW plasmas before but only with large wires and low input energy. The scattered light provided a sensitive way of locating traces of unvaporized material.

A pressure of 5×10^{-5} Torr was used to avoid the strong scattering produced by the unvaporized core. There was no evidence of current shunting at this low pressure and in fact the rf noise produced with the absence of shunting provided one of the major experimental problems.

A. Streak photographs and pinching

Three examples of streak photographs and the corresponding emission spectra are shown in Fig. 3. They illustrate the nonreproducibility of the pinching which is also reflected in the emission spectra (note different time scales). The bursts of continuum in the emission spectra occurred at the same time as the increased emission and plasma constriction in the streak photographs.

Total current in the discharge circuit was monitored with a Rogowski coil. Figure 4 shows current traces and the photodiode signals for the third example in Fig. 3. The I and dI/dt traces were quite repeatable except for the temporal position and behavior of the dI/dt perturbations. The small initial spike in dI/dt seemed to be associated with the time necessary to ionize the wire. Its time duration was proportional to the square of the wire diameter.

The current flowing in the plasma column was related to a temperature by balancing magnetic, kinetic, and inertial forces at the plasma surface as follows:

$$\frac{B^2}{2\mu}=n_e kT_e+n^T kT_i-\frac{1}{2\pi r_p}\frac{d}{dt}(\pi r_p^2 n^T m_i \dot{r}_p). \tag{1}$$

The various parameters are defined as follows: B is the azimuthal magnetic field at the column surface,

$$B=\mu I/2\pi r_p=0.2\,I/r_p\ (\mathrm{G}), \tag{2}$$

I is the plasma current inside r_p (A), r_p is the plasma column radius (cm), $\mu=4\pi$ (abH/cm), m_i, the ion mass, $=11.5\times10^{-24}$ (g), n^T is the number density of neutrals plus ions (cm^{-3}),

$$n^T=n^0+n^+ +n^{++}+n^{+++}\equiv n_e/\hat{Z}, \tag{3}$$

$\hat{Z}$ is degree of ionization, kT, the kinetic temperature (erg), $=1.60\times10^{-12}\theta$, and θ is the kinetic temperature (eV). Mass conservation between the wire and plasma

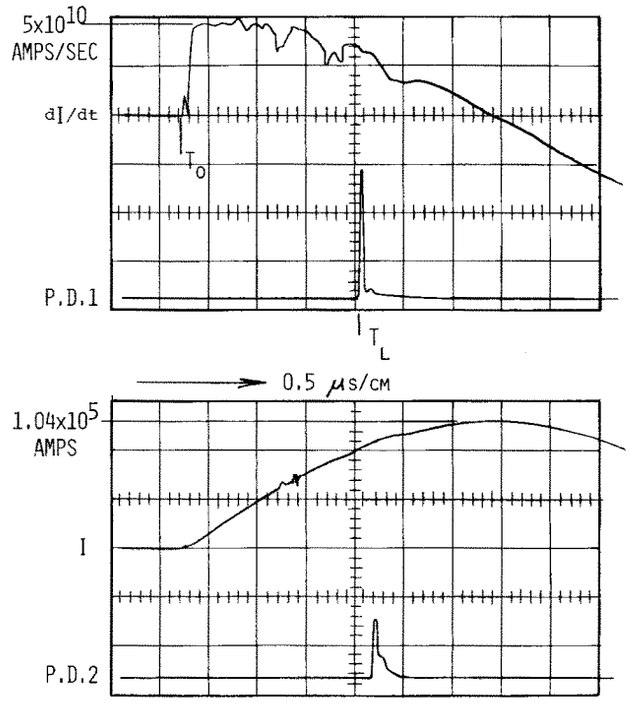

FIG. 4. Rogowski coil and photodiode signals for the third example in Fig. 3.

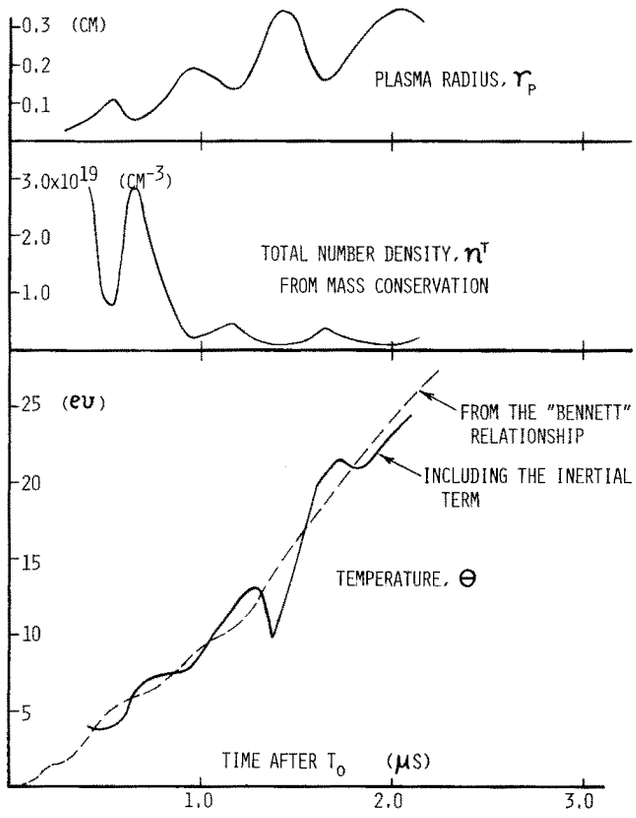

FIG. 5. Plasma column radius as measured from the third example in Fig. 3 gives n^T through mass conservation and θ from Eq. (2).

with a uniform density across the plasma column gives

$$M = \text{mass per unit length} = \text{constant}$$
$$= n^T m_i \pi r_p^2 = \rho\pi(\tfrac{1}{2}d)^2, \tag{4}$$

where ρ, the mass density of lithium, $= 0.534$ g/cm^3, d is the original wire diameter (cm), and N is the number of neutrals, ions, and electrons per unit length,

$$N = (M/m_i)(1+\hat{Z}). \tag{5}$$

With equal ion and electron temperatures, the balance equation reduces to the following form:

$$I^2 = 200NkT - 100Mr_p\ddot{r}_p. \tag{6}$$

The plasma radius was measured from the streak photograph and the second derivative was extracted numerically. The third streak photograph in Fig. 3 was used as an example, and the various measured and derived quantities from that experiment are shown in Fig. 5.

The determination of N in Eq. (6) is somewhat complicated by the fact that electron density depends on the degree of ionization and thus the temperature. The assumption of LTE and therefore Saha equilibrium leads to an iterative process which fortunately converges rapidly as described in Sec. III B.

The first two terms in Eq. (6) constitute the well-known Bennett relationship which is plotted in Fig. 5. The oscillations between 0 and 10 eV correspond to the three ionization stages which the plasma passes through as it is heated. When the third term in Eq. (6) is included in the calculation, additional oscillations in temperature result because of the plasma pinching.

Spitzer's relationship for plasma resistivity[16] gives a sufficiently large value (about 10^{-3} Ω cm) that one might expect a fairly uniform current distribution across the plasma column. The pinching model represented by Eq. (1) balances pressures only at the plasma surface as in the "snowplow" current sheath[17,18] but it also assumes that all the plasma mass is initially in this sheath. In some sense, this approximated a uniform current distribution and also resulted in a manageable description. Approximately the same final results were obtained with two other pinching models that were modified to include the effect of kinetic pressure. These were the independent particle model[19] and the snowplow model.

B. Time-resolved emission spectra

Figure 6 is higher dispersion spectrum covering some of the same wavelength region as the spectra in Fig. 3. The remainder of the visible spectrum extending to 6900 Å is shown in Figs. 7 and 8. One striking feature is the lack of any impurity lines up to the time of disrup- of the plasma column. Table I lists all the lines observed during this "stable" phase of the discharge. Many were not seen in every experiment and some were seen only once in the six spectra shown here.

LTE was assumed for all spectral analyses since the necessary condition for complete LTE specified by Griem[20] was satisfied in the region of interest for all but the ground state of Li II. This requires

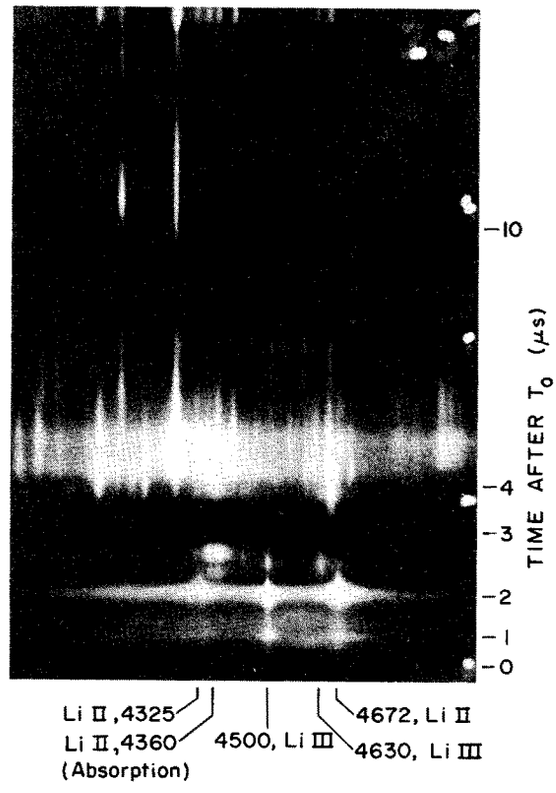

FIG. 6. Time-resolved emission spectrum from 3900 to 5000 Å. The region of interest is the first 3 μsec during which only lithium lines are seen. After 3 μsec many carbon and copper lines appear.

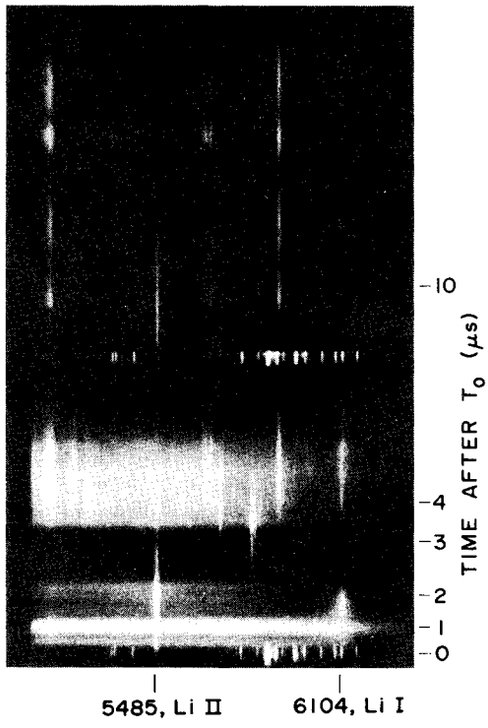

FIG. 7. Time-resolved emission spectrum from 5100 to 6200 Å.

$$n_e \geq 9\times 10^{17}(E_2/E_H)^3(kT/E_H)^{1/2}, \quad E_H = 13.6 \text{ eV}. \tag{7}$$

For LiI, $E_2 = 1.85$ eV, and the condition reduces to $n_e \geq 6\times 10^{14}\theta^{1/2}$ which is well satisfied for densities on the order of 10^{18} cm^{-3} and temperatures of a few eV. For LiII, $E_2 = 59.02$ eV, and we have the condition, $n_e \geq 2\times 10^{19}\theta^{1/2}$, which is not well satisfied for this plasma. This implies that radiative deexcitation may be an important consideration in the lower level populations. The condition for equilibrium between levels higher than the ground state is not so demanding and it is well satisfied.

These LTE conditions are for a steady-state plasma so we must ensure that relaxation times are much less than characteristic times for change in the plasma. This is certainly true in our case for translational equilibrium at densities greater than 10^{17} cm^{-3}.

The energy levels of lithium are easily available except for the upper levels of LiII. The latter were calculated by fitting the Ritz formula to the lower levels[21] and the results are shown in Fig. 9.

The internal partition functions for LiI, LiII, and LiIII were calculated using the upper level cutoff given by Griem: U^r is the partition function for lithium ($r=0$, neutral lithium),

$$U^r = \sum_{n=1}^{E_\infty^r - \Delta E_\infty^r} g_n \exp(-E_n/kT), \tag{8}$$

where ΔE_∞^r is the reduction of ionization energy (eV),

$$\Delta E_\infty^r = (r+1)e^2/4\pi\epsilon_0\rho_D = 1.44\times 10^{-7}(r+1)\rho_D^{-1}; \tag{9}$$

ρ_D is the Debye length (cm),

$$\rho_D = [\epsilon_0 kT/e^2 n_e(1+\bar{Z})]^{1/2} = 745\,[\theta/n_e(1+\bar{Z})]^{1/2}; \tag{10}$$

$$\bar{Z} = \sum_{r=1}^{3} Z_r^2 n^r/n_e = (n^+ + 4n^{++} + 9n^{+++})/n_e; \tag{11}$$

$e = 4.80\times 10^{-10}$ statC and $\epsilon_0 = 1/4\pi$ statF/cm, where the sum of statistical weights g in the partition function is taken over the quantum levels n.

To find the free-charge parameter $\bar{Z}$ the relative abundance of each species must be known which in turn requires a knowledge of their partition functions. A first approximation was made by assuming single ionization below $\theta = 4$ eV and total ionization above 10 eV with a smooth transition between. The relative abundance of each species was found through the Saha equilibrium:

$$n_e \frac{n^{r+1}}{n^r} = (6.04\times 10^{21}\theta^{3/2})\frac{U^{r+1}(\theta)}{U^r(\theta)}\exp\left(-\frac{E_\infty^r - \Delta E_\infty^r}{\theta}\right), \tag{12}$$

and the conservation relation:

$$n_e = n^+ + 2n^{++} + 3n^{+++} \equiv \hat{Z}n^T. \tag{13}$$

The iterative process converged quite rapidly and the smoothed internal partition functions for lithium in LTE between 0.1 and 100 eV are shown in Figs. 10–12. The results check with the tables of Drawin and Felenbok[22] in the limited regions of overlap. The relative abundance of each ionization stage versus temperature for an electron density of 10^{17} cm^{-3} is shown in Fig. 13. Negative lithium ions were not included in the analysis although they should be present for temperatures below the binding energy of 0.6 eV.[23]

The results of Griem were used to calculate line intensity ratios. For lines from the same ionization stage the appropriate relation is

$$\frac{I'}{I} = \frac{\lambda^3 g' f'}{\lambda'^3 g f}\exp\left(-\frac{E'_u - E_u}{kT}\right), \tag{14}$$

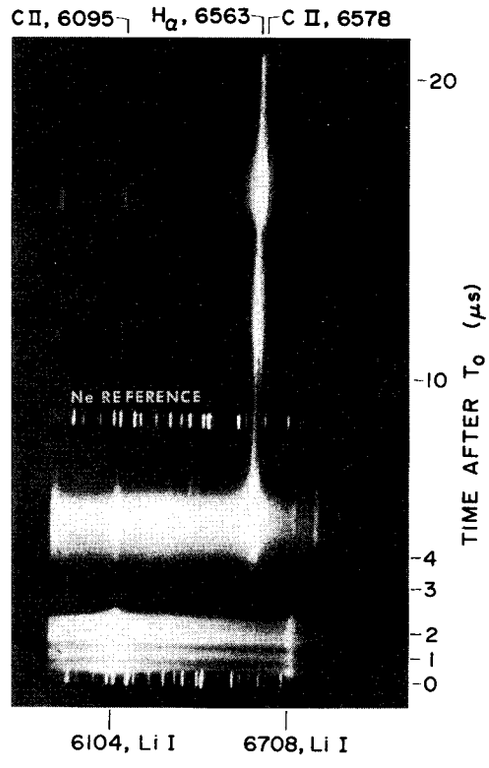

FIG. 8. Time-resolved emission spectrum from 5900 to 6900 Å.

TABLE I. Spectroscopic data for observed lines.

Element and state	λ_{air} Å	$k=1/\lambda_{vac}$ (cm^{-1})	E_u-E_1 (eV)	E_u (eV)	f[a]	g_1
Li I	6708	14900	1.848	1.85	0.753	2
Li I	6104	16380	2.031	3.88	0.667	6
Li II	5484	18230	2.260	61.28	0.308	3
	4980	20080	2.489			
Li II	4881	20480	2.539	71.90	0.085	9
Li II	4789	20880	2.588	72.23	0.654	3
Li II	4672	21400	2.653	72.23	1.01	15
Li II	4580	21830	2.706	74.96		3
Li III	4500	22220	2.754	117.55		
Li II	4360	22930	2.843			
Li II	4325	23120	2.866	72.23	0.508	9
Li I	4273	23400	2.901	4.75	0.0042	6

[a]W. Wiese, M. Smith, and B. Glennon, *Atomic Transition Probabilities*, Vol. I, *Hydrogen Thru Neon*, Report No. NSRDS-NBS 4 (U.S. GPO, Washington, D.C., 1966).

where I is the radiation intensity of the total line (W/cm² sr), λ is the vacuum wavelength of the line, f is the oscillator strength for the transition, and E_u is the energy of the upper state of the transition. The results for three line ratios appear in Fig. 14.

For relative line ratios from subsequent ionization stages we have

$$\frac{I'}{I}=\frac{\lambda^3 g' f'}{\lambda'^3 g f}(4\pi^{3/2}a_0^3 n_e)^{-1}\left(\frac{kT}{E_H}\right)^{3/2}\exp\left(-\frac{E'_u+E_\infty-E_u-\Delta E_\infty}{kT}\right), \tag{15}$$

where the primed quantites refer to the higher stage of ionization and

$$4\pi^{3/2}a_0^3E_H^{3/2}=0.167\times10^{-21}\ \text{cm}^3\,\text{eV}^{3/2}.$$

Two such line ratios are shown in Fig. 15.

Stark broadening of the 6104-Å Li I line and the 4325- and 4881-Å Li II lines was easily observable at densities of 10^{18} cm^{-3}. The full width at half-maximum for these lines was used to obtain an approximate electron density which could be compared to the density inferred through mass conservation. Line shapes were not fitted. The tables of Griem were used for the various broadening parameters and Fig. 16 shows the expected FWHM versus electron density for five lines.

The time resolution of the spectra was limited to about 0.3 μsec so the line intensity ratios and broadening would not be expected to follow any oscillations due to pinching. The accuracy of the line intensity ratios was also limited by the relative intensity of continuum emission from the plasma. In cases where there was little background to contend with, such as at 2 μsec in Fig. 17, the densitometer tracings yielded intensity ratios with an estimated standard deviation of ± 10% for the stronger lines. This results in a temperature uncertainty of less than ± 0.2 eV for the 4672/5485 ratio in the range of interest. With strong continuum however, it was sometimes difficult to extract the relative line intensitites for even the stronger lines. Errors of as much as a factor of 2 in the intensity ratio could result by cutting off the line wings.

One contradiction of the LTE assumption in the emission spectra was the 6104/6708 intensity ratio which consistently fell between 10 and 20, whereas the maximum equilibrium ratio is 3.5. This implies a potentially useful population inversion between the $3d$ and $2p$ levels of neutral lithium. As noted earlier, the equilibrium criteria which ensure dominance of collisional over radiative effects are hardest to satisfy for the ground state. In addition there were three Li II lines ($n=4$ to 3) which were compared to the prominent 4672-Å Li II line ($4f$ to $3d$, triplet). They gave intensity ratios (4672/4881, 4326, 4789) which were sometimes larger than the calculated equilibrium maximum by as much as a factor of 10. Two other ratios involving the 4672-Å line (4672/5485, 4273) gave reasonable and consistent temperatures of 4 or 5 eV. The implication is that the other $n=4$ levels were underpopulated with respect to the ^3F state. The lack of equilibirum in these upper Li II states is in violation of the usual equilibrium criteria.

Figure 17 shows the temperatures obtained from two line ratios taken from the first example in Fig. 3. Another ratio used for temperature measurements was 5485/6104. Temperatures obtained from these three ratios were between 3 and 6 eV and remained fairly constant during the first 2 μsec of the discharge. Failure of the temperatures determined from line intensity ratios to follow the gradual increase in temperature given by the Bennett relationship can be explained in several ways.

The Bennett relationship would not be a valid model if there was a uniform current distribution across the column as noted previously. Rapid field diffusion into

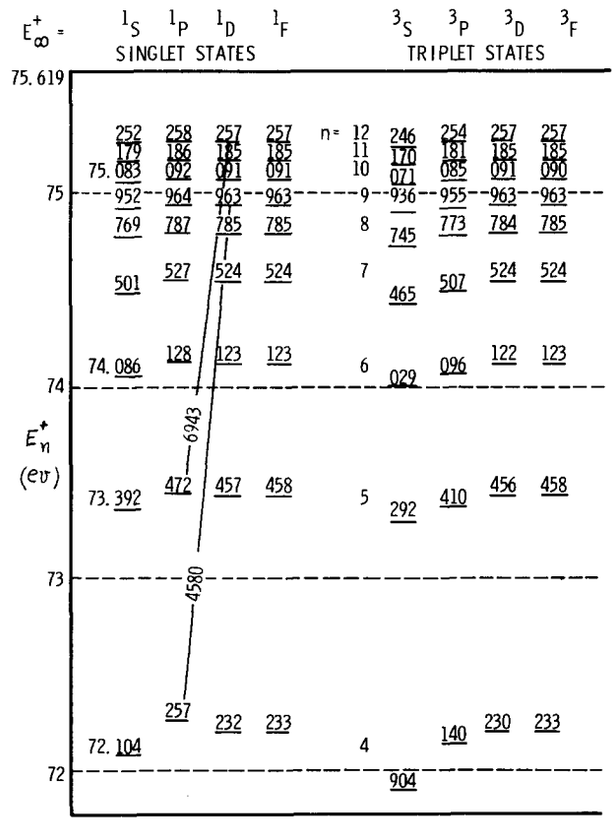

FIG. 9. Upper-state energy levels of Li II calculated by fitting the Ritz formula to the lower levels.

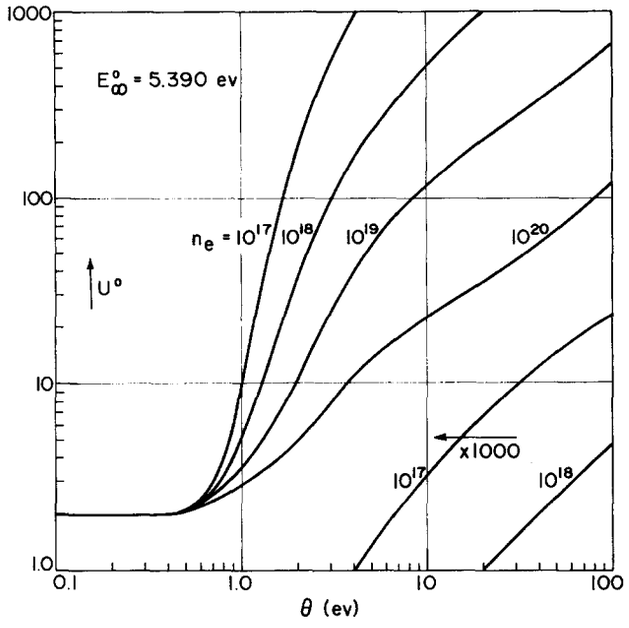

FIG. 10. Internal partition function for neutral lithium in LTE as a function of temperature and density.

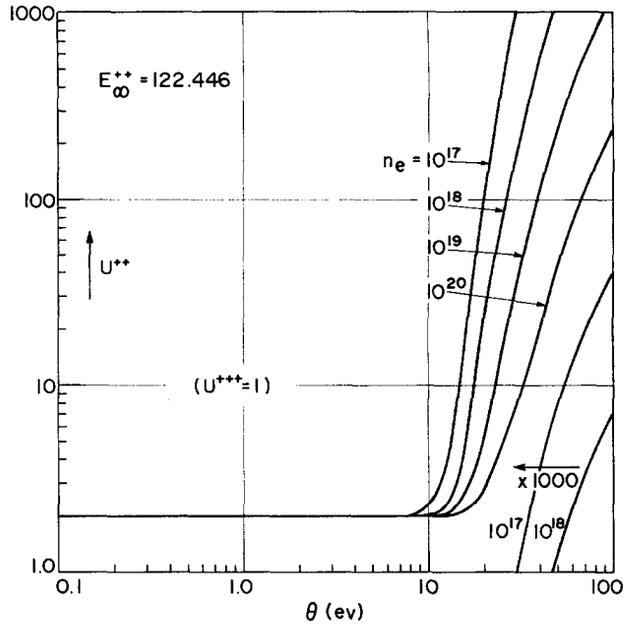

FIG. 12. Internal partition function for doubly ionized lithium in LTE as a function of temperature and density.

the plasma would also invalidate the Bennett model. A simple calculation of the expected diffusion rate gave a time of $\frac{1}{2}$ μsec for a distance equal to the plasma radius.[17]

It is possible that the lower temperatures given by the line ratios relate to the outer layers of a "thick" plasma There was occasional self-absorption in the neutral lines, for example the 6104-Å line in Fig. 18, but it usually occurred after the distinct plasma column disrupted.

The largest uncertainties in the line intensity ratios occurred at times of maximum continuum and minimum column radius. This is also the time at which Eq. (6) gave the highest temperatures so the true discrepancy is difficult to establish.

Figure 17 also shows the total density from mass conservation and the electron density from widths of the 4325- and 4881-Å lines. These were the only lines available in this region of the spectrum for broadening analysis, and in this example they were sufficiently intense for only a short time. Generally, the Li I 6104-Å line provided a much better determination of electron density. The 6104-Å line in Fig. 8, for example, gave $n_e = 1.4 \times 10^{18}$ cm^{-3} from 0.2 to 2.0 μsec, and then it dropped rapidly to 3×10^{17} at 2.4 μsec. The 6104 broadening compared to total density from mass conservation

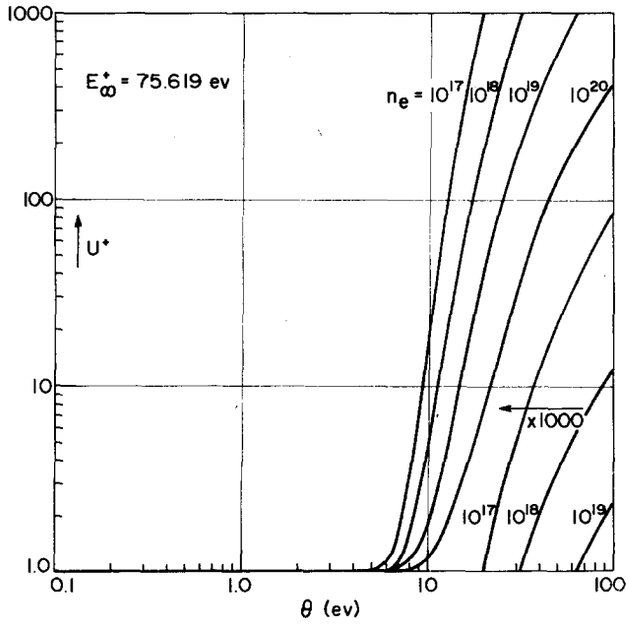

FIG. 11. Internal partition function for singly ionized lithium in LTE as a function of temperature and density.

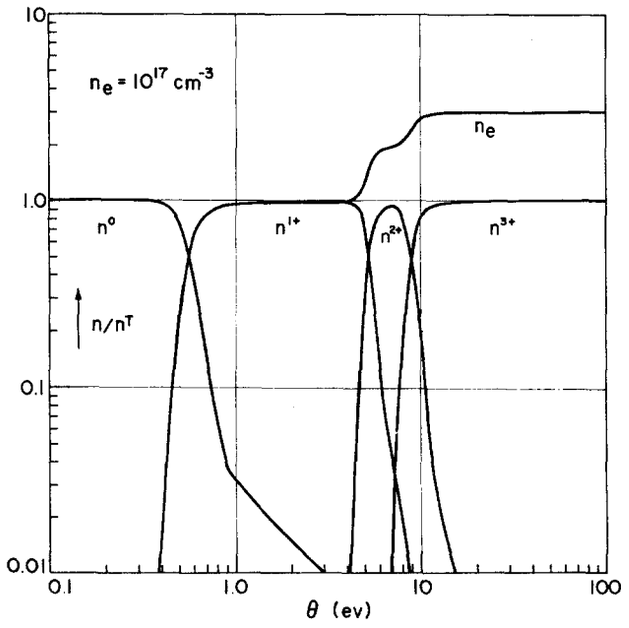

FIG. 13. Saha equilibrium distribution of lithium ionization stages vs temperature at an electron density of 10^{17} cm^{-3}.

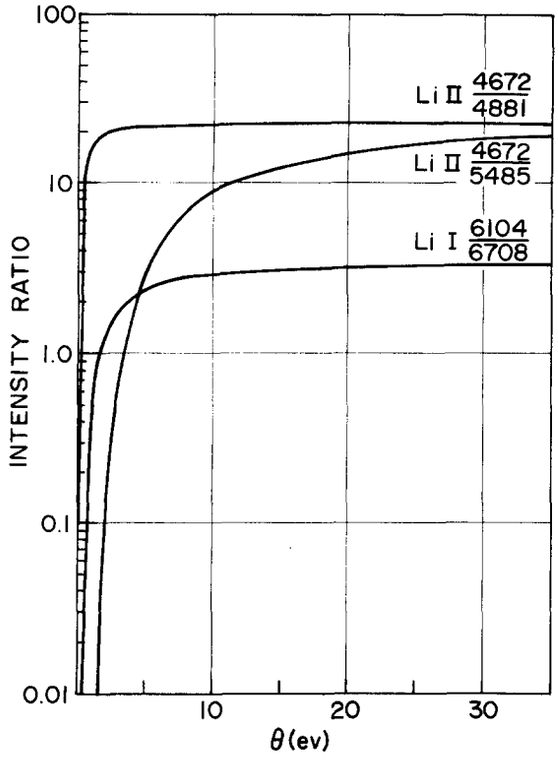

FIG. 14. Line intensity ratios vs temperature for lines from the same ionization stage.

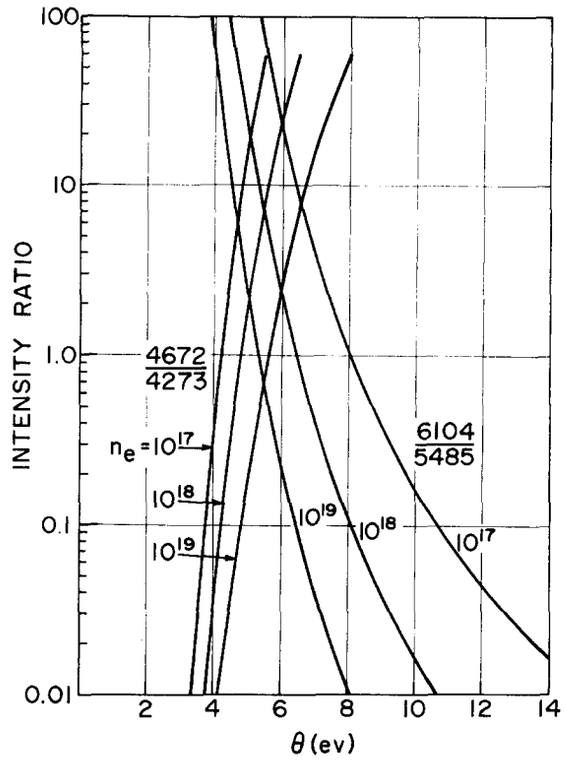

FIG. 15. Line intensity ratios for lines from subsequent ionization stages as a function of temperature and electron density.

gave $Z \approx 2$. From Fig. 13, we see that this implies $\theta = 7$ eV.

One emission line which proved difficult to identify was the strong sharp line at 4500 Å. The most likely explanation seems to be an Li III transition from $n = 5$ to 4.[24,25] Consideration was given to the possibility of doubly excited neutral lithium as the source of this line. A search was made for the doubly excited line at 3714 Å and it was not seen. Its absence does cast some doubt on the presence of a substantial doubly excited population in this plasma.[26] One other line which could be interpreted as an Li III transition appears in Fig. 6. This was an $n = 13$ to 6 transition at 4630 Å. The experimental resolution was not sufficient to study the fine structures of these lines.

There have been recent reports concerning longitudinal plasma oscillations giving rise to satellite lines related to forbidden transitions.[27–29] This possibility was considered in all of the line identifications but no satellites were found.

A short focal-length lens (70 mm) was installed inside the vacuum chamber to focus the laser to a smaller area in an attempt to affect the temperature, but no changes were seen in the spectra.

C. Light scattering

The original intent of the light scattering studies was to obtain a measure of the plasma temperature and density. The somewhat unexpected occurrence of the strong Fresnel reflection at the interface masked the weaker Thompson scattered light. Discrimination in wavelength was not possible because the low temperature did not provide sufficient broadening. Spatial discrimination was impossible because of the small and unpredictable diameter of the plasma column in interesting situations.

Figure 18 is an example of an interface reflection seen on a streak photograph along with the corresponding time-resolved emission spectrum. Three more examples are shown in Fig. 19. In all cases the early part of the column expansion cannot be seen in the reproduction so it was outlined by the dotted lines. The wires in these examples were 0.075 cm in diameter

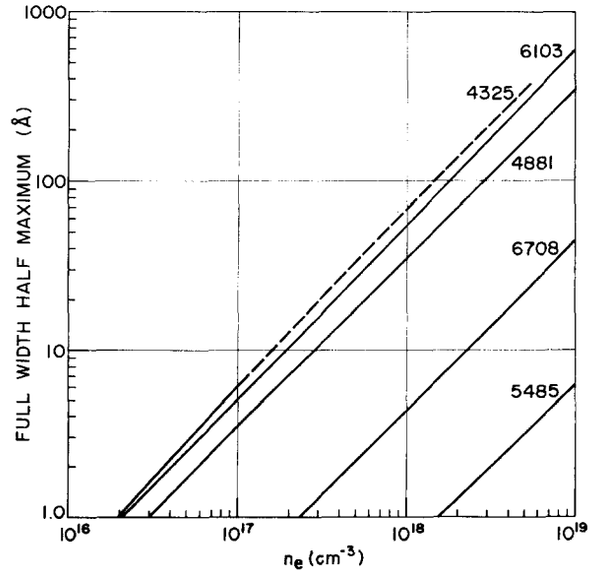

FIG. 16. Full width at half-maximum due to Stark broadening for various lithium lines.

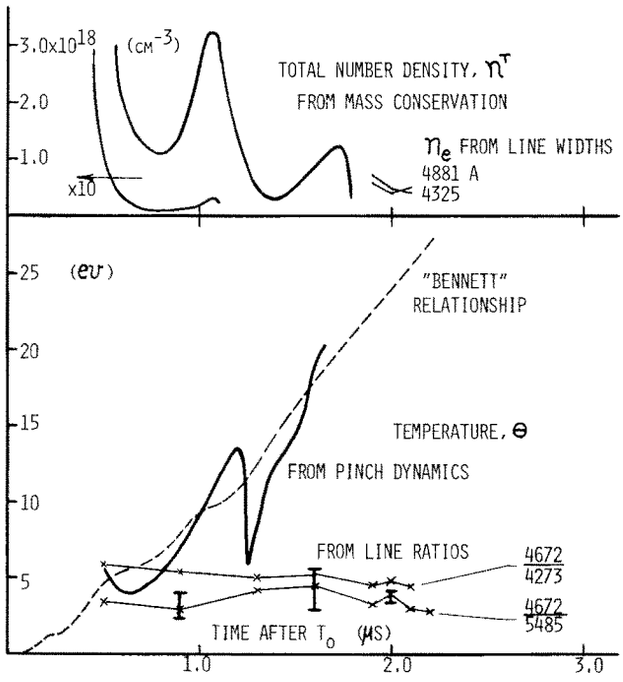

FIG. 17. Total number density and temperature for the first example in Fig. 3.

since the larger plasma diameter which resulted from a larger wire facilitated observation of the interface effect.

The position of the spectrometer entrance slit with respect to the plasma column is shown on the streak photograph in Fig. 18. The scattered ruby laser light which enters the spectrometer can be seen on the time-resolved spectrum. Spectra such as these were used to look for broadening or shifting of the scattered light.

The wires used in the experiment shown in Fig. 3 were 0.025 cm in diameter and the smaller plasma diameter and pronounced piching are evident. This strong pinching resulted in electron density fluctuations which in turn made the scattered light intensity more erratic and more difficult to study. The scattering from a plasma produced with a 0.0025-cm-diam wire was also generally weaker than with a 0.0075-cm-diam wire and at the limit of detectability with the ICC and 3000 ASA negative film used. For this reason the five-channel photomultiplier fiber-optics detector was used in conjunction with the spectrometer to observe the scattered light.

Although there were occasions when the scattered light appeared to be broadened and the intensity was consistent with Thompson scattering, these measurements could not be reliably repeated. In general the scattered light showed no broadening or shift in wavelength and the intensity required an unreasonably large electron density if interpreted as Thompson scattering.

A quantitative estimate of the Fresnel reflection coefficient was made by assuming an infinite density gradient at the vacuum-plasma interface. The scattering geometry and vertically polarized laser output allow us to consider only the Fresnel equation for the scattered light polarized perpendicular to the plane of incidence. With the incident, refracted, and reflected components denoted by i, r, and s, respectively, the reflection coefficient is given by[30]

$$R = (E_s/E_i)^2 = \sin^2(i-r)/\sin^2(i+r). \tag{16}$$

Using Snell's law and the real part of the index of refraction in the plasma given by[20]

$$n_2 = (1-\omega_p^2/\omega^2)^{1/2}, \tag{17}$$

where the plasma frequency is

$$\omega_p = 5.64\times10^4 n_e^{1/2}\ \text{sec}^{-1}, \tag{18}$$

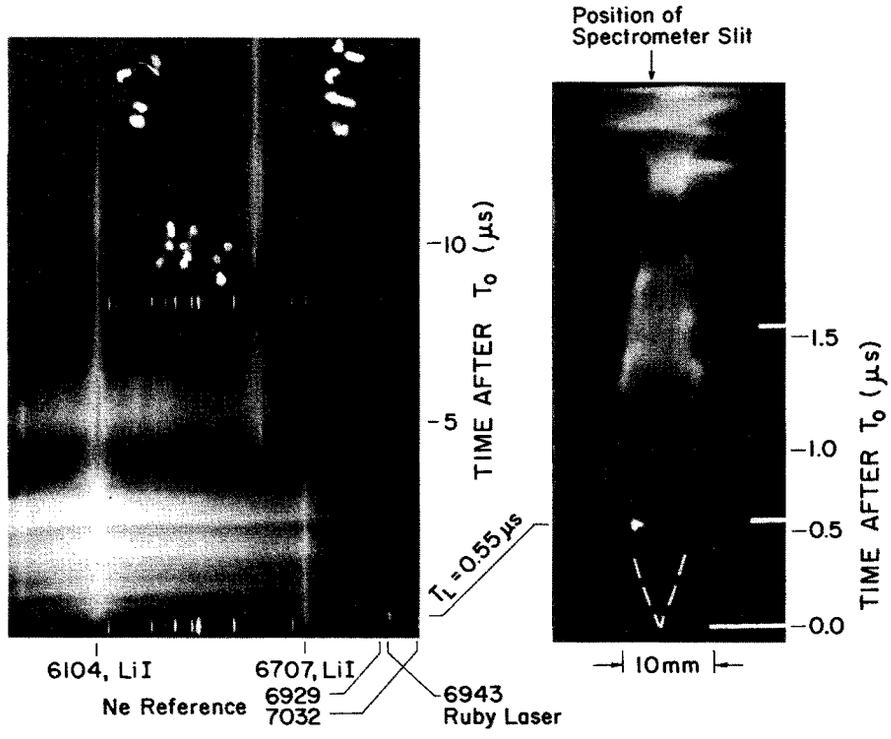

FIG. 18. Emission spectrum and the corresponding streak photograph showing the scattered light. The wire diameter was 0.0075 cm and the pressure was 5×10^{-5} Torr.

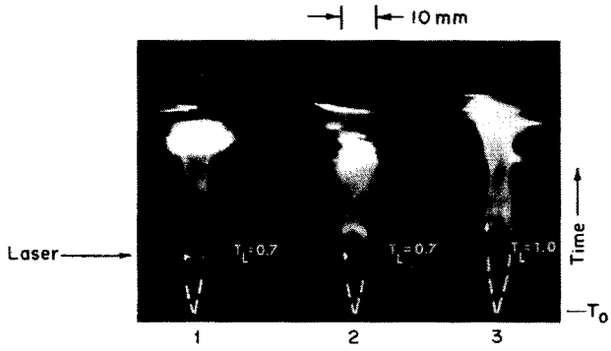

FIG. 19. Three examples of the laser-plasma interaction at the column edge. The wire diameter was 0.0075 cm and the pressure was 5×10^{-5} Torr.

and for densities sufficiently below the critical density for a ruby laser (2.33×10^{21} cm^{-3}) simple approximations give

$$n_1/n_2 \approx 1 + 2.16\times10^{-22}n_e \equiv 1+\delta, \tag{19}$$

and further trigonometric approximations yield a final result

$$R \approx \delta^2(1/4\cos^4 i), \quad \delta \ll 1. \tag{20}$$

Geometrical considerations taking into account the spectrometer acceptance angle and slit width, and the plasma column diameter showed that about 4% of the incident laser beam area could be viewed by the diagnostic optics. This resulted in a scattered power ratio of

$$P/P_0 \approx 0.2\times10^{-44}n_e^2. \tag{21}$$

An equivalent electron density for Thompson scattered light was found by calibrating the detection system through Rayleigh scattering in nitrogen gas at 760 Torr. The spectral distribution of Thompson scattered light was calculated using Salpeter's results.[31] Cooperative effects dominated because of the high density and low temperatures and the ion line was usually expected to be less than 1 Å wide. The equivalent electron density could be referred to an absolute scattered ratio by estimating the system sensitivity. The absolute system response found by estimating the photomultiplier sensitivity compared well with that obtained through geometrical considerations.

Figure 20 summarizes the scattering results from the various plasmas discussed earlier. The upper scale is the fraction of the laser light scattered into the detection system with Rayleigh scatter and stray light levels marked. The ranges shown for the two wire sizes represent many individual shots. Considering the variation of electron densities given by mass conservation and line broadening, the Fresnel reflection model readily explains the scattering results. Thompson scattering would require unreasonably high electron densities, although the possibility of a high-density sheath should not be discounted. Recent preliminary numerical calculations for these exploded wires have, in fact, shown a tendency toward strong sheath development.[32] A more selective and more sensitive detection system with a resolution better than 1 Å would permit viewing the broadened Thompson scattered light in spite of strong reflection. This could possibly provide some experimental correlation with collisional scattering theory[33–35] because of the high densities obtainable at relatively low temperature. A more repeatable plasma would facilitate seeing the electron satellites; however, the expected signal/noise ratio in this particular plasma was calculated to be close to unity even with an unbroadened satellite. A cursory search was made for the higher-frequency satellite but it was not seen.

One very remote possibility for explaining the strong scattering is selective excitation by the ruby laser.[36] There are, in fact, several transitions in lithium near 6943 Å with the $12d$-$5p$ transition in the Li II singlet state at exactly 6943 Å. Considering perturbation of the upper state energy levels, it would seem that there could have been strong absorption of the laser light.

IV. SUMMARY

A "clean" lithium plasma with electron densities as high as 10^{19} cm^{-3} and temperatures of about 4 eV was produced by exploding a thin wire at a pressure of 5×10^{-5} Torr. The necessity of using a pressure less than 10^{-3} Torr to eliminate an unvaporized core in the plasma resulted in a short-lived plasma column with little temporal repeatability. There appeared to be no current shunting and all of the wire was vaporized and ionized within 100 nsec.

If the scattered light was interpreted as electron scattering, the electron densities required were much higher than those given by mass conservation and Stark broadening. Mass conservation gave electron densities between 10^{17} and 10^{19} cm^{-3} as the plasma column oscillated in size and these matched the Fresnel reflection model very well.

This problem of interface reflections obscuring the electron scattering will have to be dealt with in all scattering diagnostics on high-density plasmas. It has already been seen with laser-produced plasmas. If the temperature is high enough, the ion line will be wider than the nondispersed Fresnel reflection; and if the plasma is repeatable, the electron features (plasma satellites) could be found. Unfortunately, the effect of collisions is to narrow the ion line and broaden the sattelites, which makes their detection more difficult. Spatial discrimination will prove difficult since high-density plasmas are usually small in size.

No repeatable broadening or wavelength shift was seen

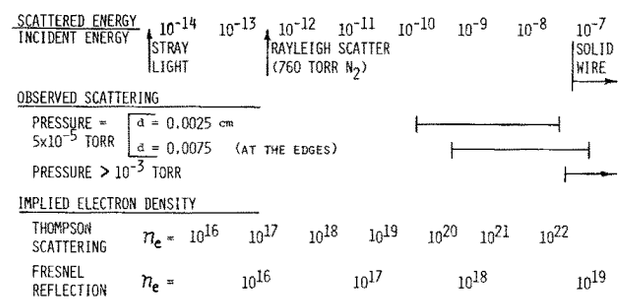

FIG. 20. Summary of observed scattered intensities and comparison with scattering models.

in the scattered light greater than the instrumental resolution of 1 Å, but results were complicated by mode hopping of the laser. The average temperature of 4 eV measured by emission line ratios implied an expected ion feature which was not quite wide enough to be seen (FWHM = 1.1 Å at 10^{18} cm^{-3}) outside the much stronger Fresnel reflection. An unsuccessful attempt was made to find an electron satellite, although they were expected to be so weak as to be nearly buried in the plasma emission.

There were occasional streak photographs which showed scattering at the column center and not at the edges such as in Fig. 3. This happened so rarely that a quantitative comparison with Rayleigh scattering was not obtained, but rough comparisons of film densities gave an electron density equivalent to that obtained from mass conservation if interpreted as Thompson scattering. The Bennett distribution for density in a linear discharge is peaked at the center,[18] so there are no contradictions in ascribing this center scattering to cooperative electron scattering. The absence of Fresnel reflection in these cases implies a smaller density gradient at the plasma boundary.

There were no impurity lines in the emission spectra until disruption of the plasma column at about 2 μsec. Several of the lithium emission lines did not have intensities consistent with LTE even though the usual LTE criteria were satisfied, and in fact there were indications of a population inversion. Three separate line intensity ratios consistently gave an equilibrium temperature of about 4 eV, however, time resolution did not allow following short-term variations due to pinching. In fact, the bursts of continuum and pinch dynamics implied short-term rises in temperature when the column was pinched.

There appear to be no previous reports of observation of the Li III emission line at 4500 Å. Its occurrence in this EW plasma provides an opportunity for a spectroscopic study of its fine structure. Only one other Li III line appeared and it was seen only once (4630 Å). Most of the strong Li III emission lines lie in the ultraviolet, but ultraviolet techniques and equipment were not available for this study.

*Work supported in part by the Air Force Office of Scientific Research.
†Based in part upon a thesis submitted by T. A. Leonard to The University of Michigan for which partial support was obtained from the National Aeronautics and Space Administration and the United States Atomic Energy Commission.
‡Present address: KMS Fusion, Inc., P. O. Box 1567, Ann Arbor, Mich. 48106.
[1]S. A. Ramsden, Phys. Rev. Lett. **13,** 227 (1964).
[2]H. Weichel, *Eighth Conference on Phenomenon in Ion Gases* (Springer-Verlag, Vienna, 1967), p. 524.
[3]Y. Iyawa, Jap. J. Appl. Phys. **7,** 954 (1968).
[4]C. Wang, Phys. Rev. Lett. **26,** 823 (1971).
[5]H. Rohr, Z. Phys. **209,** 295 (1968).
[6]E. Oktay and D. R. Bach, J. Appl. Phys. **41,** 1716 (1970).
[7]P. Cabannes, C.R. Acad. Sci. (Paris) **263,** 360 (1966).
[8]V. Scherrer, *Exploding Wires* (Plenum, New York, 1968), Vol. 4, p. 137.
[9]R. Tomlinson, IEEE J. Quantum Electron. **5,** 591 (1969).
[10]N. Ahmad, B. Gale, and M. Key, J. Phys. B **2,** 403 (1969).
[11]M. Daehler, J. Appl. Phys. **38,** 1980 (1967).
[12]T. A. Leonard, Rev. Sci. Instrum. **39,** 1374 (1968).
[13]T. A. Leonard, Rev. Sci. Instrum. **40,** 964 (1969).
[14]T. Korneff, *Exploding Wires* (Plenum, New York, 1959), Vol. 1, p. 104.
[15]R. Maninger, Ref. 14, p. 156.
[16]L. Sptizer, *Physics of Fully Ionized Gases* (Interscience, New York, 1962).
[17]D. Rose and M. Clark, *Plasmas and Controlled Fusion* (MIT Press, Cambridge, Massachusetts, 1965).
[18]S. Glasstone and R. Lovberg, *Controlled Thermonuclear Reaction* (Van Nostrand, New York, 1960).
[19]S. Gartenhaus, *Elements of Plasma Physics* (Holt Rinehart and Winston, New York, 1964), p. 43.
[20]H. Griem, *Plasma Spectroscopy* (McGraw-Hill, New York, 1964).
[21]H. E. White, *Introduction to Atomic Spectra* (McGraw-Hill, New York, 1934).
[22]H. Drawin and P. Felenbok, *Data for Plasmas in Local Thermodynamic Equilibrium* (Gauthier-Villars, Paris, 1965).
[23]B. Ya'akobi, Phys. Lett. **23,** 655 (1966).
[24]This transition was pointed out by Gordon Drake, University of Windsor.
[25]J. D. Garcia and J. E. Mack, J. Opt. Soc. Am. **55,** 654 (1965).
[26]J. Bromander (private communication).
[27]M. Baranger and B. Moyer, Phys. Rev. **123,** 25 (1961).
[28]G. V. Zelenin, Sov. Phys.-JETP **31,** 1009 (1970).
[29]B. Ya'akobi and G. Bekefi, Phys. Lett. A **30,** 539 (1969).
[30]M. Born and E. Wolf, *Principles of Optics* (Pergamon, New York, 1965).
[31]E. E. Salpeter, Phys. Rev. **120,** 1528 (1960).
[32]D. Chapin and J. J. Duderstadt (private communication).
[33]D. DuBois and V. Gilinsky, Phys. Rev. A **133,** 1308 (1964).
[34]E. Leonard (private communication).
[35]E. J. Linnebur and J. J. Duderstadt (private communication).
[36]R. M. Measures and A. B. Rodrigo, Appl. Phys. Lett. **20,** 102 (1972).